Supporting Information

Spectroelectrochemical Approaches to Mechanistic Aspects of Charge Transport in *meso Nickel (II) Schiff* Base Electrochromic Polymer

Kamila Łępicka,[a] Piotr Pieta,*[a] Aleksander Shkurenko,[a] Paweł Borowicz,[a] Marta Majewska,[a] Marco Rosenkranz,[b] Stanislav Avdoshenko,[b] Alexey A. Popov,*[b] and Wlodzimierz Kutner[a,c]

[a]Institute of Physical Chemistry, Polish Academy of Sciences, Kasprzaka 44/52, 01-224 Warsaw, Poland

[b]Leibniz Institute for Solid State and Materials Research, Dresden (IFW Dresden), Helmholtzstrasse 20, D-01069 Dresden, Germany

[c]Faculty of Mathematics and Natural Sciences, School of Sciences, Cardinal Stefan Wyszynski University in Warsaw, Wóycickiego 1/3, 01-815 Warsaw, Poland

The *meso*-SaldMe ligand does not polymerize because two phenol moieties are labile in a supporting electrolyte solution and, therefore, they can repel each other, that way increasing distance between them.

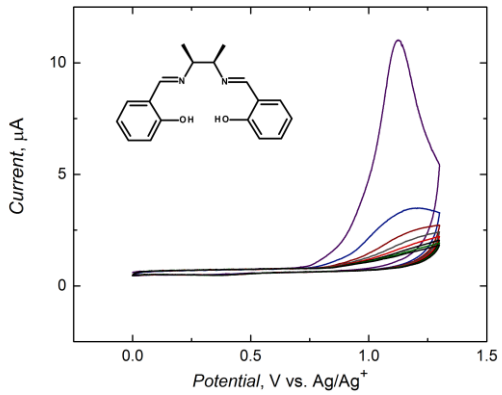

Figure S1. The CV curve for 0.1 mM *meso*-SaldMe ligand in the acetonitrile solution of 0.1 M (TBA)ClO_4 recorded during anodic potential scanning. The potential scan rate was 50 mV s^{-1}. Inset shows the structural formula of the *meso*-SaldMe ligand.

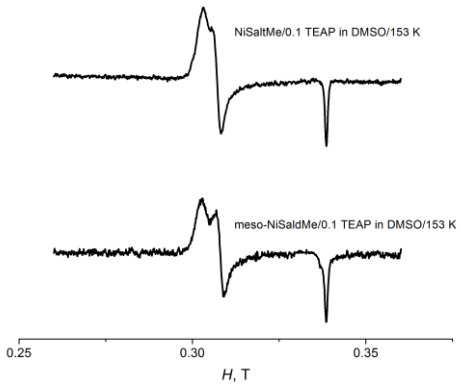

Figure S2. Low-temperature (T = 150 K) ex situ ESR spectra of one-electron oxidized Salen-monomers in 0.1 M (TEA)ClO_4 in DMSO at 153 K.

Spectroelectrochemical properties of oxidized Salen monomers were dependent on the solvent nature. We did not observe characteristic ESR signals for Ni(III) in acetonitrile, which is a moderately electron-donating solvent but we did observed signals characteristic of Ni(III) in electron-donating solvents, e.g., DMSO. In DMSO, we enforced the Ni(II)/Ni(III) electro-oxidation but we blocked polymerization of the Ni(II)Salen complex. The low-temperature ex situ ESR spectra (Fig. S2) of NiSaltMe and *meso*-NiSaldMe exhibited signals characteristic of an axially symmetric S=1/2 Ni(III)-Schiff base complexes.
(*meso*-NiSaldMe; g1=2.2596, g2=2.2223, g3=2.0205)
(NiSaltMe; g1=2.2577, g2=2.2290, g3=2.0214)

The Uv-vis spectra recorded (Fig. S3) did not change significantly with the change of the potential applied, thus indicating no change in the electronic structure of the polymer.

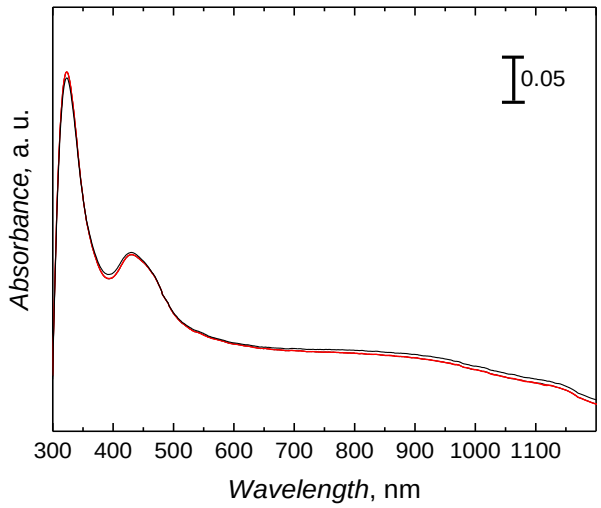

Figure S3. The UV-vis absorption spectra for poly[*meso*-Ni(II)-saldMe] in the acetonitrile solution of 0.1 M $(TBA)ClO_4$ recorded during anodic potential sweeping under cyclic voltammetry conditions. Spectra were recorded in the potential range of 0.0 to 0.40 V vs Ag/Ag^+.

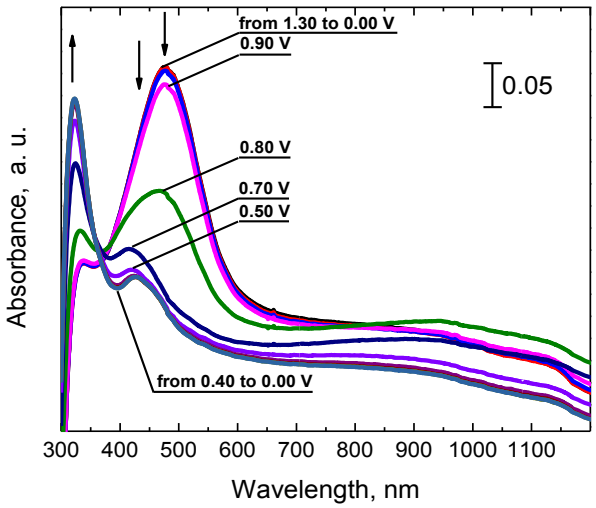

Figure S4. UV-vis absorption spectra of poly[*meso*-Ni(II)-SaldMe] in the acetonitrile solution of 0.1 M $(TBA)ClO_4$ recorded during cathodic (backward) potential scanning under CV conditions in the potential range of 1.30 to 0 V vs Ag/Ag+ at the scan rate of 5 mV s^{-1}.

Computational studies

Optimization of parameters

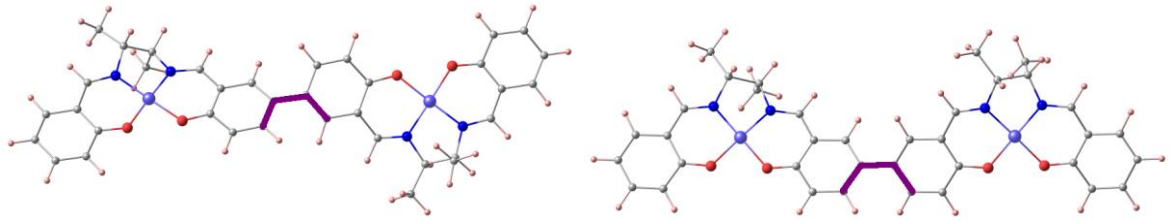

Scheme S1. DFT-optimized *trans* and *cis* isomers of the *meso*-Ni(II)-saldMe dimer. The highlighted in purple dihedral (twist) angles are 34° and 37°, and inter-monomer bonds are 1.480 Å and 1.481 Å for the *trans* and *cis* isomer, respectively. The *trans* isomer is by 2 kJ/mol more stable than the *cis* isomer. Presumably, *cis* and *trans* monomers are randomly distributed in a real polymer.

Positive charging exerts a clear but not dramatic effect on the inter-monomer interaction. In the dimer, the inter-monomer bond length is 1.469 and 1.458 Å in the mono and dication, respectively, and the inter-monomer dihedral angle is decreased to 30° (cation) and 21° (dication). Thus, there is a certain tendency of assuming a quinoid structure with the charge increase. However, this structure is still far from reaching the true double bond character for the inter-monomer bond. In the longer oligomers, the effect of positive charging is weaker and its nature is more complex. Namely, there is a tendency to "localize" charge on dimer fragments, particularly pronounced for dications. In the singly-charged trimer, both inter-monomer bonds are shortened to 1.473 Å and the dihedral angle is decreased to 32°. However, one of the inter-monomer bonds is further decreased to 1.463 Å with dihedral angle of 26° in the dication, whereas another inter-monomer bond becomes 1.486 Å long with the dihedral angle of 45°. In the tetramer, there is a similar tendency. That is, the middle inter-monomer bond slightly increases with the charge increase (1.482 and 1.484 Å in the mono- and di-cation, respectively) with concomitant increase of the dihedral angle (39 and 42°), whereas two other inter-monomer bonds are shortened (1.474 and 1.467 Å in the +1 and +2 state, respectively) with the analogous decrease of the dihedral angle (32° and 28° in the +1 and +2 state, respectively). Noteworthy, this "alteration" effect reminds Peierls' distortion of the one-dimensional lattice.

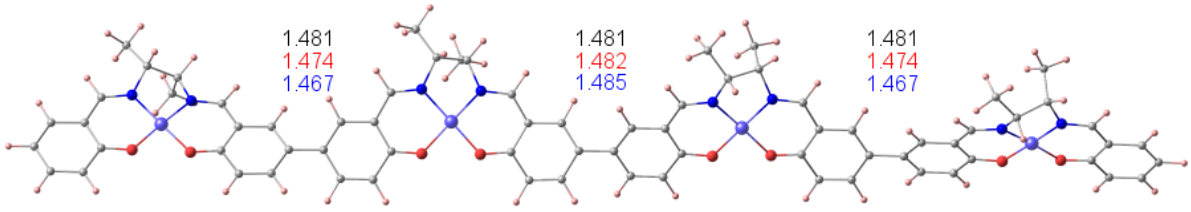

Scheme S2. Inter-monomer bond lengths in tetramer in the neutral (black), cationic (red), and dicationic (blue) states.

Band structure calculations for the neutral and charged polymer

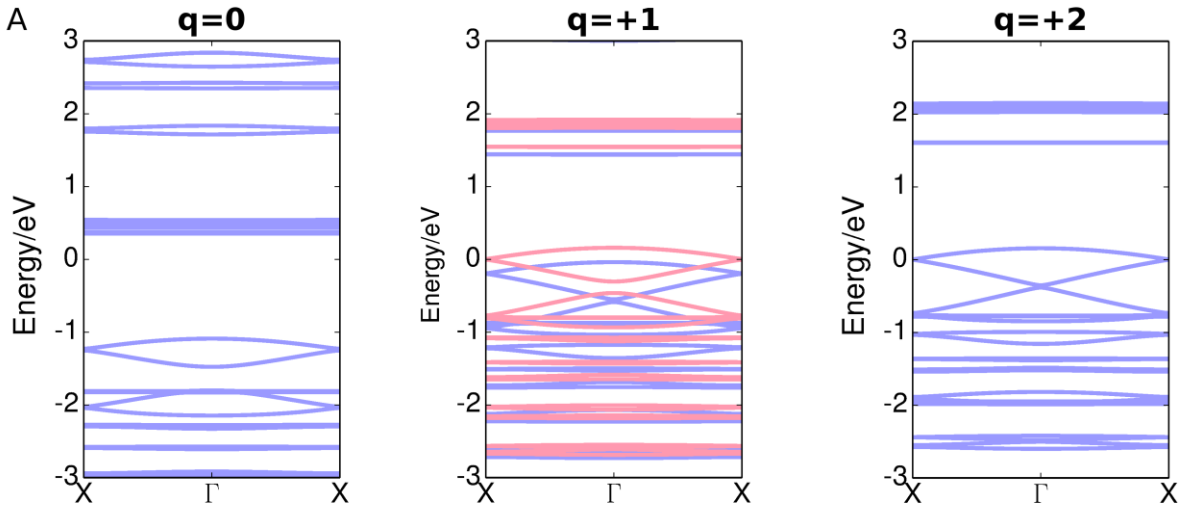

Figure S5. The band structure of the neutral polymer and of its charged states with the +1 and +2 charge on the repeat unit. Notably, calculations predict a metallic state for the charged polymer.

Charged states – TD-DFT calculations

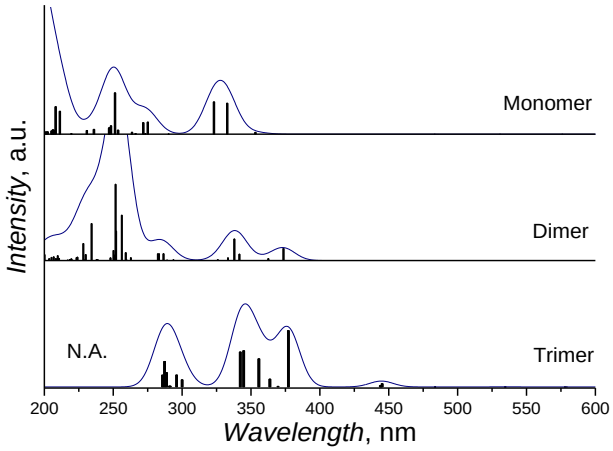

Figure S6. Excitation spectra of the neutral monomer, dimer, and trimer computed at the TD-DFT level (CAM-B3LYP/def2-SVP). Notably, high-energy excitation states of the trimer are not accessible within the range of computed values.

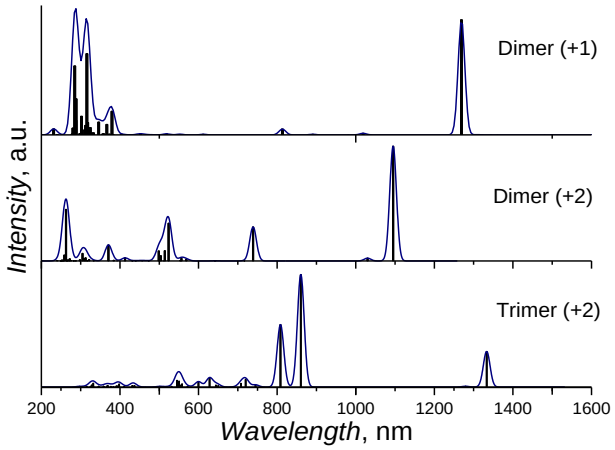

Figure S7. Excitation spectra of the charged dimer (+1 and +2 states) and trimer (+2 state) computed at the TD-DFT level (CAM-B3LYP/def2-SVP). Computations for charged states yielded transition in the low-energy (long wavelength) range with unrealistically high intensities. Analysis of these transitions showed that they have large contribution from intra-molecular electron transfer along the oligomer chains. Such excitations are not physical with respect to the real polymer. Based on these results, we conclude that computations for charged oligomers are not much reliable and, therefore, cannot be used for analysis of experimental spectra.

Computations of IR spectra

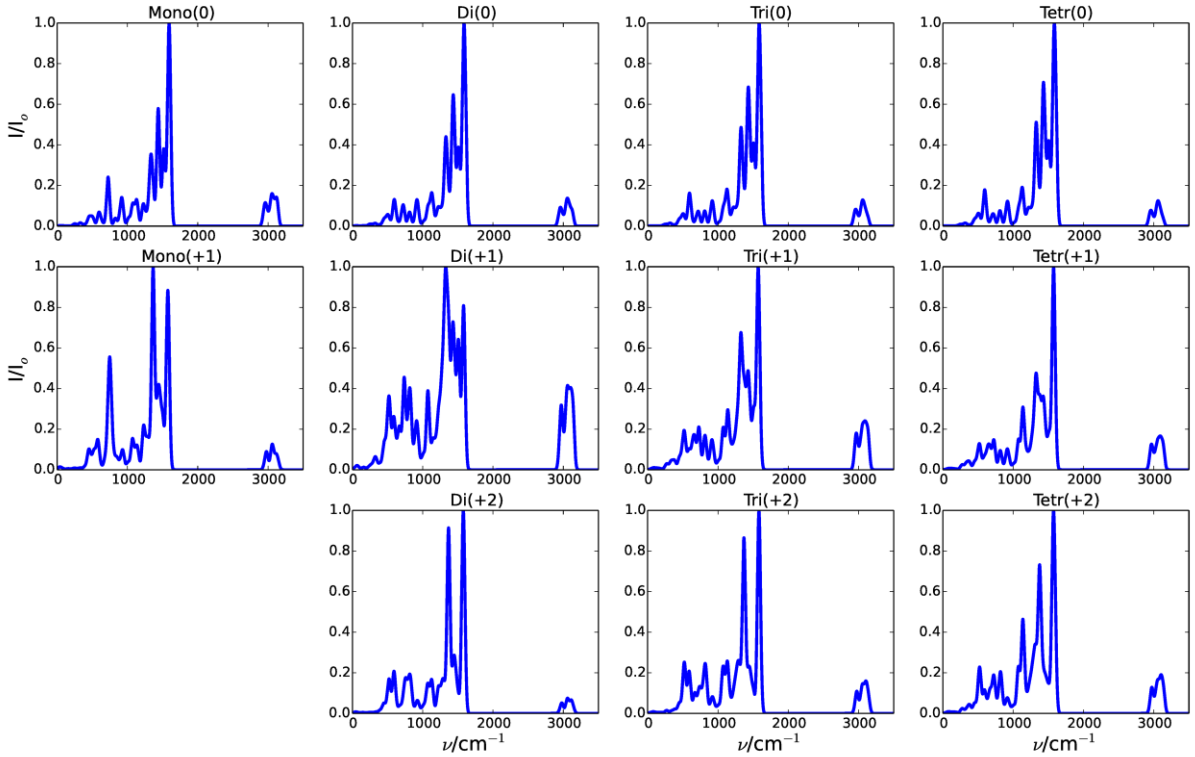

Figure S8. The IR spectra calculated for *meso*-Ni(II)-saldMe oligomers of 1 to 4 monomer length and the charge 0, +1, and +2.

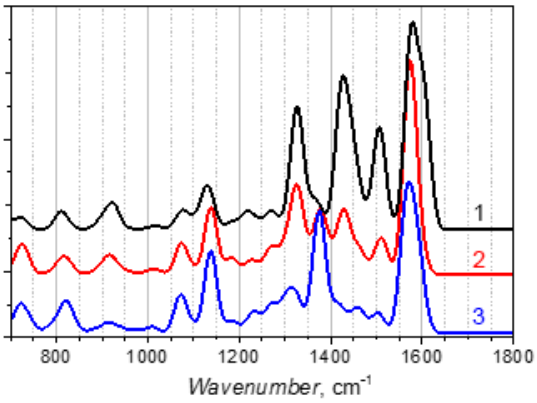

Figure S9. Computed IR spectra of the *meso*-Ni(II)-saldMe tetramer in the (1) 0, (2) +1 and (3) +2 charged state.

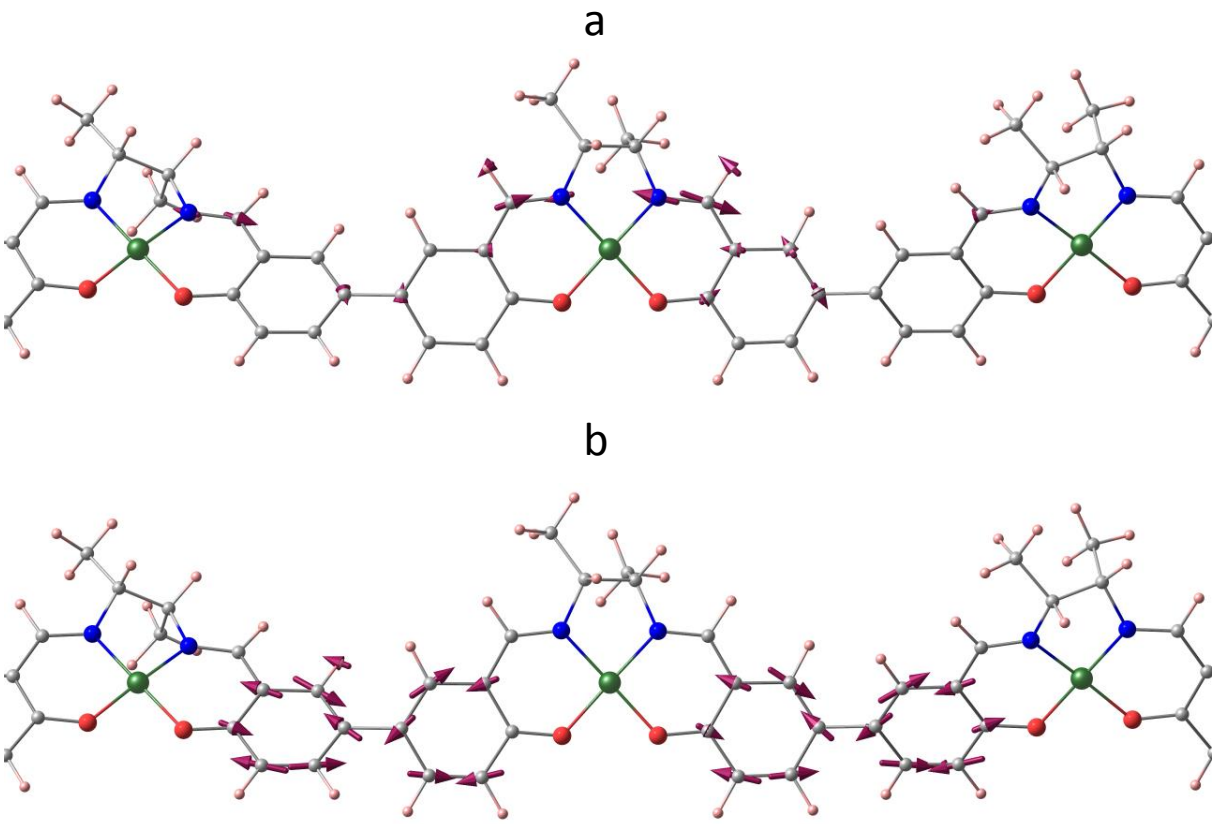

Scheme S3. The structural formula of the *meso*-Ni(II)-SaldMe oligomer showing (a) predominantly C=N stretching vibration (calc. 1574 cm^{-1}) and (b) predominantly phenyl-based vibration (calc. 1607 cm^{-1}).

Synthesis of *meso*-*N,N'*-bis-(salicylidene)-2,3-butanediaminonickel(II), *meso*-Ni(II)-SaldMe

Chemicals and reagents

All reagents used for synthesis of *meso*-*N,N'*-bis(salicylidene)-2,3-butanediaminonickel(II), *meso*-Ni(II)-saldMe, i.e., dimethylglyoxime, lithium aluminium hydride (LAH), salicylic aldehyde, acetate tetrahydrate [$Ni(OAc)_2 \cdot 4H_2O$], anhydrous potassium carbonate (K_2CO_3), magnesium sulfate ($MgSO_4$), anhydrous solvents and solvents of HPLC grade were from Sigma-Aldrich. Commercial diethyl ether was dried over freshly activated (for at least 24 h at 250 °C) 3Å molecular sieves for at least three days.

Instrumentation

NMR spectra were recorded at room temperature with a Varian Gemini Dual spectrometer (200 MHz ^{1}H, 50 MHz ^{13}C). Chemical shifts (δ) are reported in ppm relative to Me_4Si (δ 0.00) or D_2O δ 4.79) for ^{1}H and residual chloroform (δ 77.00) for ^{13}C. The following abbreviations were used to indicate signal multiplicity: s - singlet; d - doublet; q - quartet; m - multiplet. High resolution mass spectra (HRMS) were recorded using the electron impact (EI) ionization method with a Waters AutoSpec Premier spectrometer. Melting points were measured with Opti Melt automated melting point apparatus MPA100. X-ray diffraction data were collected at 100.0(1) K on an Agilent SuperNova diffractometer equipped with a Mo-Kα micro-focus X-ray source, X-ray mirror optics and Eos CCD detector. Experimental temperatures were regulated using an Oxford Cryosystems open-flow nitrogen cryostat. The data were processed with CrysAlis Pro program package (Agilent Technologies, 2014) typically using an empirical multi-scan absorption correction with the SCALE3 ABSPACK routine. Crystal structure was solved by a direct method using SHELXS-97 program and refined by the full-matrix least-square method on F^2 with anisotropic displacement parameters for non-hydrogen atoms using the SHELXL-2013 program within the WinGX single crystal X-ray diffraction program system.

Preparation of *meso*-Ni(II)-SaldMe

meso-Ni(II)-SaldMe was synthetized according to the following three-step procedure.

1st step. Synthesis of *meso*-2,3-diaminobutane dihydrochloride 1 by dimethylglyoxime reduction

Excessive amount of lithium aluminium hydride (2.96 g, 0.078 mol) was added to a solution of dimethylglyoxime (3.03 g, 0.026 mol) in anhydrous diethyl ether (250 mL) by small portions at 0 °C. Then, the mixture was stirred at room temperature for two days under an argon atmosphere. After that time, the mixture was cooled to -78 °C and quenched by addition, in the following order, samples of 3 mL of water, 3 mL of 15% NaOH, and 9 mL of water. The resulting mixture was warmed to room temperature and stirred for 4 h, then dried with K_2CO_3, and then filtered through the pad of Celite®. The solvent was gently removed under decreased pressure. The residue was neutralized with 1 M HCl (5 eq., 130 mL) and the solution was evaporated to dryness by azeotropic distillation with toluene to yield 3.31 g of crude products. Next, the products, *meso*-2,3-diaminobutane dihydrochloride and DL-diaminobutane dihydrochloride, were separated by fractional crystallization from methanol. The DL-diaminobutane dihydrochloride is more soluble (7 g per

100 mL MeOH at 22 °C) than the *meso*- isomer. After separation, 1.62 g of *meso*-2,3-diaminobutane dihydrochloride was obtained.

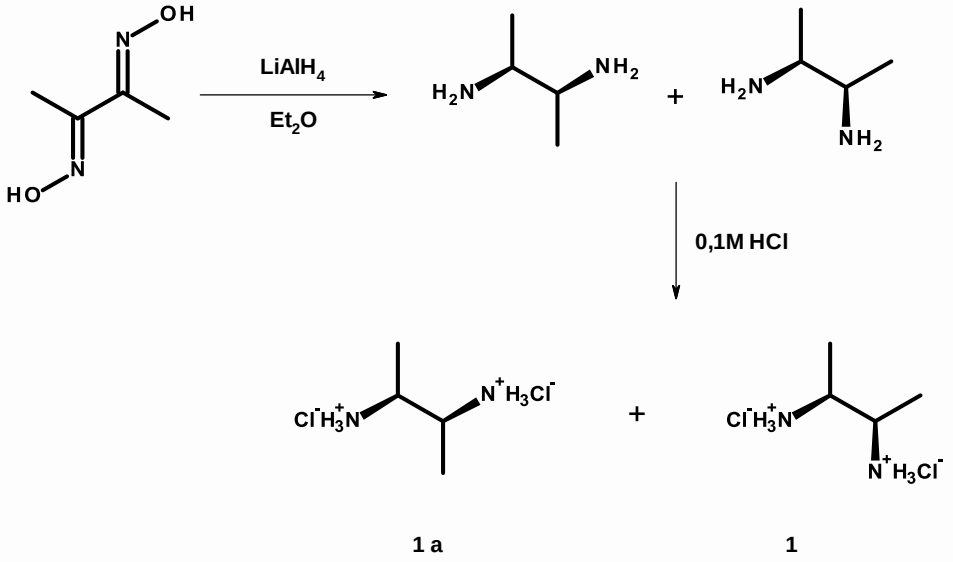

1 a **1**

Scheme S4. Reaction equation for synthesis of DL-diaminobutane dihydrochloride **1a** and *meso*-2,3-diaminobutane dihydrochloride **1**.

Structure of **1** was confirmed by ^{1}H NMR and ^{13}C NMR spectroscopy. The NMR (^{1}H NMR, $CDCl_3$) spectra of **1**:

- ^{1}H NMR (D_2O) δ 1.49 (d, 6H, C<u>*H*</u>$_3$CH); 3.75 (q, 2H, CH$_3$C<u>*H*</u>)
- ^{13}C NMR (D_2O) δ 14.72 (<u>*C*</u>H$_3$CH); 49.97 (CH$_3$<u>*C*</u>H). Two signals were detected, as expected.

2nd step. Synthesis of *meso-N,N'*-bis(salicylidene)-2,3-diaminobutane 2

A water (4 mL) solution of **1** (0.56 g, 3,5 mmol) and K_2CO_3 (1.06 g, 7.7 mmol) was stirred for 20 min. Then, ethanol (25 mL) was added to the reaction mixture, and then the mixture was heated to 60 °C. Next, freshly distilled salicylic aldehyde (0.85 g, 7 mmol) was added in one portion and the reaction mixture was heated under reflux for 6 h. After cooling to room temperature, the solvent was removed under decreased pressure and the residue dissolved in chloroform. Subsequently, the solution was washed with water, then dried with $MgSO_4$, and then concentrated. The product was recrystallized from dichloromethane and hexane (1.01 g, yield 98%).

Melting point of **2** was 121-124 °C

The NMR spectra of **2**:

- ^{1}H NMR ($CDCl_3$) δ 1.26 (d, 6H, C<u>*H*</u>$_3$CH); 3.48 (q, 2H, CH$_3$C<u>*H*</u>); 7.08 (m, 8H, arom); 8.38 (s, 2H, N=C<u>*H*</u>PhOH); 13.29 (s, 2H, PhO<u>*H*</u>)
- ^{13}C NMR ($CDCl_3$) δ 19.90 (s, CH<u>*C*</u>H$_3$); 70.09 (s, CH<u>*C*</u>H$_3$); 117.43 (arom); 119.15 (arom); 131.90 (arom); 132.82 (arom) 161.48 (PhOH); 164.73 (N=<u>*C*</u>HPhOH).

High resolution mass spectrometry (HRMS). Calculated and obtained *m/z* for $C_{18}H_{20}N_2O_2$ was 296.1524 and 296.1523, respectively.

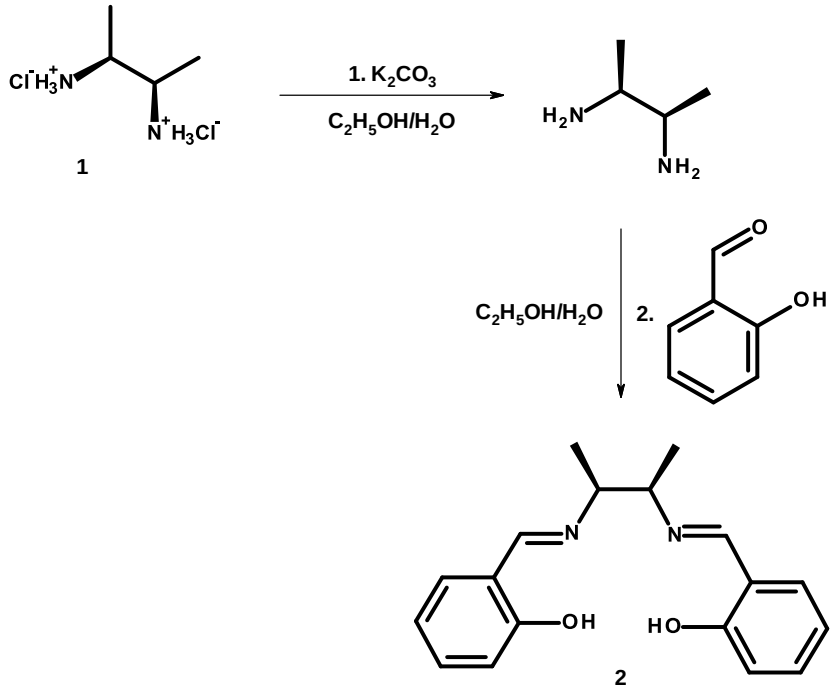

Scheme S5. Reaction equation for synthesis of *meso-N,N'*-bis(salicylidene)-2,3-diaminobutane **2**.

3rd step. Synthesis of *meso-N,N'*-bis(salicylidene)-2,3-butanediaminonickel(II)

K_2CO_3 (0.86 g, 6.2 mmol) and $Ni(OAc)_2 \cdot 4H_2O$ (0.77 g, 3.1 mmol) were simultaneously added to a suspension of *meso-N,N'*-bis(salicylidene)-2,3-diaminobutane (0.92 g, 3.1 mmol) in a mixture of water and tetrahydrofurane (40 mL; 1:1, *v*/*v*). The resulting mixture was stirred at room temperature for 24 h under an argon atmosphere. The residual product was filtered through a fine filter, and then washed with water until filtrate became clear. The product was recrystallized from anhydrous acetonitrile (0.87 g, yield 79.8%).

Melting point of **3** was 246-252°C.

The NMR (^{1}H NMR, $CDCl_3$) spectrum of **3**: δ 1.29 (d, 6H, CHC<u>*H*</u>$_3$); 3.59 (q, 2H, C<u>*H*</u>CH$_3$); 6.50 (t, 4H, arom); 7.0 (d, 4H, arom); 7.27 (s, 2H, N=C<u>*H*</u>PhOH).

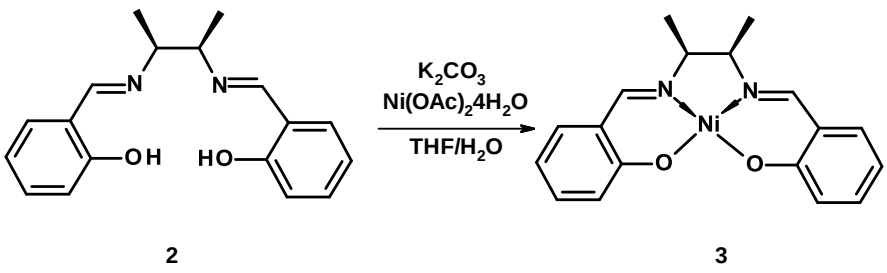

Scheme S6. Reaction equation for synthesis of *meso-N,N'*-bis(salicylidene)-2,3-butanediaminonickel(II) **3.**

Molecular structure of *meso*-*N*,*N*'-bis(salicylidene)-2,3-butanediaminonickel(II)

Table S1. Crystal structure data and collection parameters for **3.**

Empirical formula	$C_{18}H_{18}N_2O_2Ni$
Formula weight	353.05
Temperature	100.0(1) K
Wavelength	0.71073 Å
Crystal system	Monoclinic
Space group	$P2_1/c$
Cell parameters-Unit cell dimensions	a = 10.5421(3) Å
	b = 12.2460(2) Å
	c = 12.1471(3) Å
	β = 109.298(3)°
Cell Volume	1600.92(7) $Å^3$
Z*, Calculated density	4, 1.465 mg m^{-3}
Absorption coefficient	1.22 mm^{-1}
F(000) **	736
Crystal size	0.27 × 0.22 × 0.13 mm
Range for data collection θ, limiting indices	3.5–29.6°, $-14 \le h \le 14$, $-18 \le k \le 17$, $-16 \le l \le 15$
Reflections collected / unique	23597 / 4161 [R_{int} = 0.034]
Data / restraints / parameters	4161 / 0 / 210
Goodness-of-fit on F^2 GooF***	1.019
Final R indices [$I > 2\sigma(I)$]	$R1$ = 0.029, $wR2$ = 0.069
R indices (all data)	$R1$ = 0.036 , $wR2$ = 0.072
Extinction coefficient	-
ρ_{max} and ρ_{min}****	0.70 and -0.25 e $Å^{-3}$

*The number of units in elemental cell

**Structure factor at $h = k = l = 0$

***Fitting parameter

****Highest difference electron density peak

A scheme of atom numbering, ORTEP diagram, and approximate dimensions of the molecule **3** is shown in Figure S4. X-Ray structure investigations have shown that the Ni atom has a tetrahedrally distorted square planar coordination involving two O and two N atoms of the tetradentate ligand, with the *cis* configuration of

coordinated atoms. The Ni atom is located 0.0088(6) Å from the N_2O_2 coordination plane and maximum deviation from planarity of the coordinated atoms is 0.0963(6) Å.

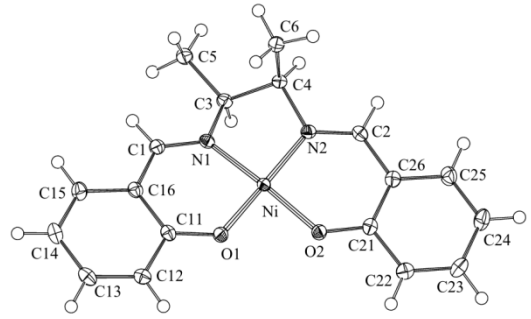

a

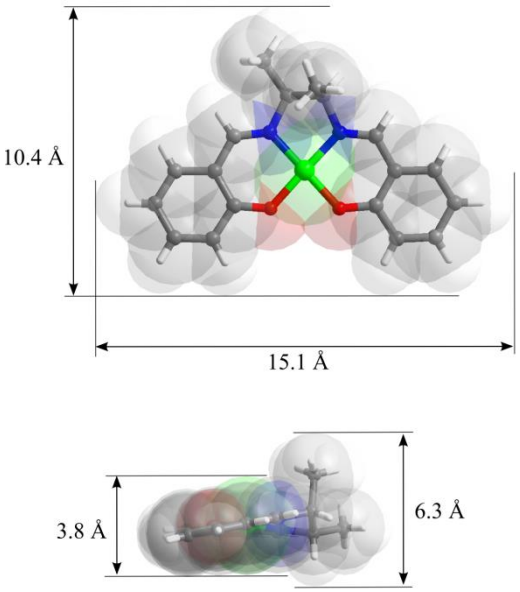

b

Figure S10. Molecular structure of **3**. (a) The ORTEP diagram with the atom numbering scheme. Ellipsoids are shown with 50% probability. (b) Approximate dimensions of the molecule with van der Waals radii are taken into account.

The configuration of **3** is *meso*, and then adopted conformation is a propeller-like deformed umbrella. The two aldehyde moieties are twisted with the dihedral angle between two (O-C_6H_4-CH=) planes equal to 9.12(5)°. Deviations of the imine carbon atoms, C3 and C4, from the NiN_2O_2 plane are -0.492(2) and 0.289(2) Å, respectively. The conformation of the imine bridge is *gauche* with the NCCN torsion angle equal to 46.2(2)°, then methyl groups of the diamines are located in pseudo-axial and pseudo-equatorial positions (Figure S4 b).